

SYNTHESIS OF CELLULOSE-BASED AEROGELS FROM BAGASSE COMBINED WITH ACTIVATED CARBON FOR ENHANCED OIL SPILL REMEDIATION

CAO MINH TRUNG,* PHAM QUOC PHU,* HA THANH TOAN,** VAN PHAM DAN THUY,* TRAN
THI BICH QUYEN,* NGUYEN VIET NHAN HOA,* YOSHIYUKI MURATA*** and
DOAN VAN HONG THIEN*

*Faculty of Chemical Engineering, Can Tho University – 3/2 Str., Ninh Kieu District,
Can Tho City, Vietnam

**Institute of Food and Biotechnology, Can Tho University, 3/2 Str., Ninh Kieu District,
Can Tho City, Vietnam

***Graduate School of Environmental and Life Science, Okayama University, Okayama, 700-8530, Japan
✉ Corresponding author: Doan Van Hong Thien, dvhthien@ctu.edu.vn

Received July 25, 2024

This study synthesized a cellulose-based aerogel from bagasse with activated carbon and tested its effectiveness for crude oil spill remediation. Scanning electron microscopy (SEM) analyzed the morphology of bagasse fibers and their integration within the aerogel. Brunauer-Emmett-Teller (BET) analysis revealed a surface area of 34.53 m²/g, a micropore volume of 0.040 cm³/g, and 96.4% porosity. The Barrett-Joyner-Halenda (BJH) plot showed predominantly mesoporous features with an average pore diameter of 28.2 Å. X-ray diffraction (XRD) indicated a crystalline structure with a 76.4% crystallinity index. Fourier-transform infrared (FTIR) spectroscopy confirmed the presence of functional groups. Thermogravimetric analysis (TGA) and differential scanning calorimetry (DSC) showed excellent thermal stability. The aerogel exhibited an oil adsorption capacity of 12.78 grams per gram in seawater, demonstrating its effectiveness in oil spill cleanup.

Keywords: activated carbon, bagasse, cellulose aerogel, oil spill

INTRODUCTION

Global environmental pollution has become an urgent issue of concern in recent years, with water pollution emerging as one of the most critical challenges. This form of pollution is driven by a multitude of contaminants that pose severe risks to human health through consumption, contact, or use of polluted water.¹ Alarmingly, more than 80% of wastewater from human activities is discharged into rivers and oceans without treatment, leading to extensive environmental degradation and the proliferation of over 50 diseases. Poor water quality is associated with 80% of diseases and 50% of child deaths globally.² Toxic pollutants in water encompass chemicals, debris, bacteria, and parasites, contributing to a public health crisis. Notably, the adverse effects of polluted and unsafe water result in more human fatalities than wars and other forms of violence combined.^{3,4}

Another significant environmental issue is oil

spills, a major concern since the 1960s caused by petroleum exploration and production on continental shelves, as well as the operation of supertankers capable of transporting over 500,000 metric tons of oil.⁵ These spills pose severe environmental threats, particularly when large quantities of oil spread over extensive areas. Interestingly, nearly half of the estimated 1 million tons of oil that enter marine environments annually originates from land-based sources, such as factories, farms, and cities, rather than from tanker spills.^{6,7} Researchers have developed various physical, chemical, and biological methods to address oil spills and remove harmful substances from polluted water. These methods include adsorption, biodegradation, filtration, flocculation, and reverse osmosis.^{8,9} Despite their utility, these techniques often face limitations, including high costs, environmental impact, complexity, and the

potential for generating secondary pollution.

Recently, a promising material known as “aerogels” has emerged as a solution to various technological and environmental challenges.^{6,7,10} Aerogels are distinguished as the lightest, strongest, and most porous solid materials available. They are produced through a process that involves substituting the liquid component of a gel with a gas, yielding a product characterized by its extremely low density and minimal thermal conductivity.^{6,7,11} Referred to colloquially as “frozen smoke”, “solid smoke”, or “blue smoke”, aerogels were first introduced by Samuel Stephens Kistler in 1931.¹² Their unique properties, including selective adsorption of oils and water, hydrophobicity, reusability, and effectiveness in oil recovery, render aerogels highly efficient sorbents for organic solvents in aquatic environments.¹¹

One type of aerogel currently receiving significant research interest is cellulose aerogel, which is synthesized using waste paper or cellulose-based materials, such as agricultural by-products.^{10,13,14} The primary structural component of these aerogels is cellulose fibers, derived from plant cell walls, making them a sustainable and eco-friendly choice.¹⁵ Despite their promise, cellulose aerogels often exhibit low surface areas because of the characteristics of the raw material and the synthesis process, which can affect their pore structure and distribution.¹⁶ To overcome these limitations and enhance the performance of cellulose aerogels, researchers have explored doping them with various chemicals to increase their surface area.^{17,18} Activated carbon (AC) is a notable additive in these studies, known for its high surface area and excellent adsorption capacity for gases, liquids, and organic molecules.¹⁹⁻²¹ The integration of AC with cellulose aerogels holds significant promise for improving their efficiency in applications such as water filtration and oil spill treatment.

This study explores the synthesis of cellulose aerogels derived from sugarcane bagasse, an agricultural by-product, with the incorporation of activated carbon to improve their adsorption properties. The objective is to advance sustainable aerogel technology by utilizing agricultural waste to develop environmentally friendly and efficient materials for water treatment and environmental remediation. The research also investigates how different parameters affect the oil adsorption capacity of the aerogels, including optimal adsorption time, temperature, salinity, and material

reusability.

EXPERIMENTAL

Materials

This study utilized sugarcane bagasse procured from Cai Rang market, Can Tho city, Vietnam, as a cellulose precursor for aerogel synthesis. Polyvinyl alcohol (PVA, Mw 89000-98000, 99% hydrolyzed), hydrogen peroxide (H₂O₂, 34.5-36.5%), and sodium hydroxide (NaOH, pellets, ≥95%) were obtained from Sigma Aldrich. Activated carbon (AC, specific surface area of 580-1100 m²/g) was imported from MICBAC, India, while silica ceramic coating powder (fumed silica) was purchased from OCI, Korea. All chemicals were employed as received without further purification.

Method

Pre-treatment sugarcane bagasse

Sugarcane bagasse (SB) was initially comminuted into small fibers (20 g) and subjected to alkaline hydrolysis process. The fibers were immersed in 200 mL of a 1 wt% NaOH solution at 100 °C for 2 hours. Subsequently, the treated bagasse was thoroughly washed with distilled water and bleached by immersion in 100 mL of a 10 wt% H₂O₂ solution for 30 minutes. The pH of the solution was adjusted to 12 through the gradual addition of 2 M NaOH. Following this treatment, the bagasse was again washed with distilled water and dried at 60 °C for 24 hours to obtain functionalized fibers.

Fabrication of cellulose-based aerogels

To prepare the PVA solution, 0.1 g of PVA was dissolved in 50 mL of distilled water and sonicated at 70 °C for 1 hour. Subsequently, 0.2 g of SB and varying amounts of AC were added to the PVA solution. The specific ratios of SB/PVA/AC are detailed in Table 1. This mixture was then stirred at 300 rpm using a magnetic stirrer for 30 minutes. The resulting gel was poured into a mold and stored in a refrigerator at -20 °C for 2 hours. After freezing, the gel was freeze-dried at -70 °C for 48 hours to obtain the aerogel. Finally, the aerogels were cured at 80 °C for 3 hours to enhance the crosslinking of PVA molecules within the material.

Hydrophobic modification of cellulose aerogels

The hydrophobic modification of cellulose aerogels was achieved through the incorporation of fumed silica to enhance surface hydrophobicity. Initially, 1 g of fumed silica was dispersed in 50 mL of ethanol and sonicated for 15 minutes to ensure uniform dispersion.

Characterization of cellulose aerogels

The cellulose aerogels (CA1, CA2) were then immersed in the suspension for 2 hours, allowing fumed silica to adhere to the aerogel surface and form a hydrophobic layer. Subsequently, the modified aerogels were dried at 60 °C for 24 hours to remove residual ethanol and stabilize the surface treatment.

Morphological analysis

The morphology of cellulose aerogels was analyzed using a scanning electron microscope (SEM, JCM-7000 JEOL). Prior to observation, the samples were coated with platinum to enhance imaging.

Specific surface area and porosity

The specific surface area and porosity of the aerogels were determined using nitrogen adsorption and desorption techniques, performed on BET equipment (Quantachrome Instruments, version 11.0). The samples were initially degassed at 300 °C for 5 hours via the nitrogen reduction method. Subsequently, they were subjected to nitrogen adsorption at -196 °C under variable pressure conditions. The specific surface area was calculated using the following equations:

$$\frac{1}{W\left(\frac{P}{P_0}-1\right)} = \frac{C-1}{V_m C} \times \frac{P}{P_0} + \frac{1}{V_m C} \quad (1)$$

$$S_{total}(\text{Surface area}) = \frac{V_m N_a \sigma \times 10^{-18}}{22.4 \times 10^3} \quad (2)$$

$$S_{BET}(\text{Specific surface area}) = \frac{S_{total}}{a} \quad (3)$$

where P is the partial vapor pressure of the adsorbate gas (nitrogen) at 77.3 K, P₀ is the saturated pressure of the adsorbate gas, W is the volume of gas adsorbed at STP to form a monolayer, V_m is the volume of gas adsorbed at STP to form a monolayer, C is a dimensionless constant related to the enthalpy of adsorption, N_a is Avogadro's constant, CCC is a dimensionless constant related to the enthalpy of adsorption, σ is the adsorption cross section, a is the mass of the adsorbent.

The porosity of the aerogel samples was determined using the following equation:

$$\emptyset = 100 \left(1 - \frac{\rho_a}{\rho_c}\right) \quad (4)$$

where ρ_a represents the density of the aerogel, and ρ_c is the density of crystalline cellulose (1.5 g/cm³).²²

Table 1
Composition of cellulose aerogel samples

Sample*	SB:PVA:AC (g)
CA1	2:1:0
CA2	2:1:0.25
CA3	2:1:0.5

*Cellulose aerogel samples prepared with different SB/PVA/AC ratios were denoted as CA1, CA2, and CA3, respectively

Crystallographic analysis

The crystal structure and nanoscale dimensions of cellulose were investigated using X-ray diffraction (XRD) with a D8 Advanced system (Bruker). The analysis was conducted over a 2θ range from 5° to 70°. The key characteristics assessed included the positions and relative intensities of the diffraction peaks, which provide insights into the material's crystal structure. The degree of crystallinity was quantified by analyzing the XRD patterns, with a focus on peak positions and their intensities. This analysis enabled the assessment of both the crystallinity and the nanoscale dimensions of the cellulose. The quantification of crystallinity was performed using the following equation:

$$CrI(\%) = \frac{\text{Area of crystalline peaks}}{\text{Area of all peaks (Crystalline+Amorphous)}} \times 100 \quad (5)$$

Functional group analysis

Fourier transform infrared spectroscopy (FTIR) was performed using a Shimadzu IRAffinity-1s WL spectrometer to identify the functional groups present in the cellulose aerogels. The FTIR spectra were obtained by scanning in the range of 4000 to 400 cm⁻¹, with each spectrum being an average of 35 scans. A spectral resolution of 4 cm⁻¹ was employed to ensure precise identification and characterization of the functional groups within the aerogels.

Thermal stability and degradation

The thermal stability and degradation characteristics of the materials were evaluated using a Thermogravimetric Analysis-Differential Scanning Calorimetry (TGA-DSC) system, specifically the STA 490PC/4/H Luxx Netzsch thermal analyzer. The analysis was performed over a temperature range from ambient conditions to 900 °C, with a controlled heating rate of 5 °C per minute. The experiments were conducted in an air atmosphere to simulate oxidative conditions and assess the materials' thermal behavior.

Oil adsorption tests

The oil adsorption capability of the aerogels was evaluated following the ASTM F726-17 standard, which outlines procedures for assessing materials' effectiveness in responding to oil spills under conditions that simulate seawater. To prepare the testing medium, Castrol Activ 4T 20W-40 motor oil was used to mimic crude oil. Seawater was simulated by preparing an aqueous solution containing 3.5% NaCl to replicate the salt content of seawater, and the pH was adjusted to 8. Motor oil was then added to this medium at a concentration of 50 g/L and uniformly dispersed. During the oil adsorption test, the aerogels were immersed in the oil-contaminated water and allowed to adsorb the oil for a specified duration. After the adsorption period, the aerogels were removed from the

water surface, dried at 100 °C to eliminate any adsorbed water, and the maximum oil adsorption capacity (Q) was calculated based on the weight of oil adsorbed.

$$Q = \frac{m_2 - m_1}{m_1} \quad (6)$$

where Q ($\text{g}\cdot\text{g}^{-1}$) is the maximum oil adsorption capacity, m_1 (g) is the initial mass of the aerogel, m_2 (g) is the mass of the aerogel after drying.

Investigation of factors affecting the oil adsorption process

To evaluate the impact of different parameters on the oil adsorption performance of the aerogels, systematic investigations were conducted. The effect of salinity was examined by varying the NaCl concentration from 2.5% to 5%, while keeping all other experimental conditions constant. Similarly, the influence of adsorption temperature was assessed over a range of 10 °C to 60 °C, and the adsorption time was varied from 10 to 90 minutes to determine its effect on oil uptake.

Reusability

The reusability of the aerogels was evaluated through a physical recovery process. In each adsorption cycle, the aerogels were immersed in oil for 30 minutes, then recovered and regenerated by heating at 100 °C for 60 minutes to remove the adsorbed oil and residual moisture. This procedure was repeated for five consecutive cycles to assess the material's durability and reusability. To ensure accuracy and reliability, each experiment was performed in triplicate. The reported values represent the mean of three independent experiments, with standard deviation included to reflect data variability.

RESULTS AND DISCUSSION

Morphology and structure of sugarcane bagasse aerogels

Figure 1 illustrates the morphology and structure of the sugarcane bagasse aerogels. Figure 1(a) presents images of cellulose aerogel (CA) samples, showing that the color of the CAs deepens with increasing carbon content. Preliminary assessments indicate that CA3 exhibits brittleness and is prone to breaking. Figure

1(b) shows the formation of cross-links between sugarcane fibers and polyvinyl alcohol (PVA). These cross-links are attributed to hydrogen bonds formed between the hydroxyl groups on the sugarcane fibers and the PVA chains.

Figure 2 displays SEM images of the cross-sectional morphology of aerogels CA1 (a), CA2 (b), and CA3 (c), highlighting their porous structures. The images reveal a 3D interconnected network of fibers forming major pores with diameters in the tens of micrometers. The pore size distribution appears non-uniform, indicating variations in the aerogel's internal architecture.

Upon the incorporation of activated carbon (CA2 and CA3), significant structural transformations are observed at both the micro and macro levels. Compared to CA1, the fibrous network in CA2 remains interconnected, preserving an open and porous structure, although with slight densification. However, in CA3, the pore structure becomes less distinguishable, with fibers appearing more aggregated and collapsed, potentially reducing the aerogel's porosity and affecting its functional properties. These morphological variations serve as key selection criteria for optimizing the activated carbon content. The primary requirement is to maintain the aerogel's structural integrity while ensuring sufficient porosity. Since CA3 exhibits excessive densification and loss of visible pores, CA1 and CA2 were selected for further investigations. Figure 3 shows the XRD patterns for the CA samples. For the CA1 sample, peaks are observed at 2θ angles of 15.26° and 22.14°, corresponding to the diffraction planes (110) and (200), respectively. Similarly, the CA2 sample exhibits peaks at 2θ angles of 16.51° and 22.51°, also corresponding to the (110) and (200) diffraction planes. Additionally, characteristic peaks of PVA appear at 19.23° in CA1 and 20.26° in CA2.

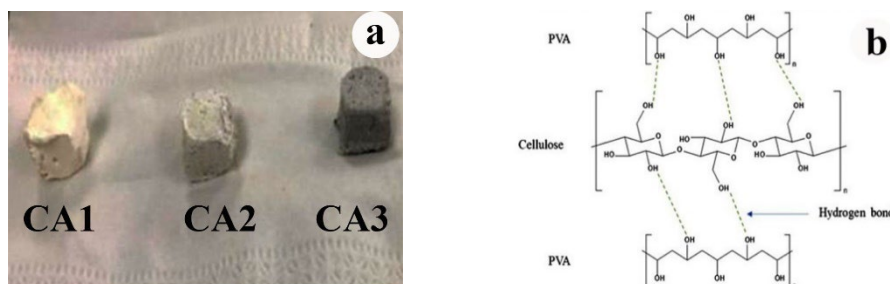


Figure 1: (a) CA samples, (b) Hydrogen bonds between cellulose and PVA polymers

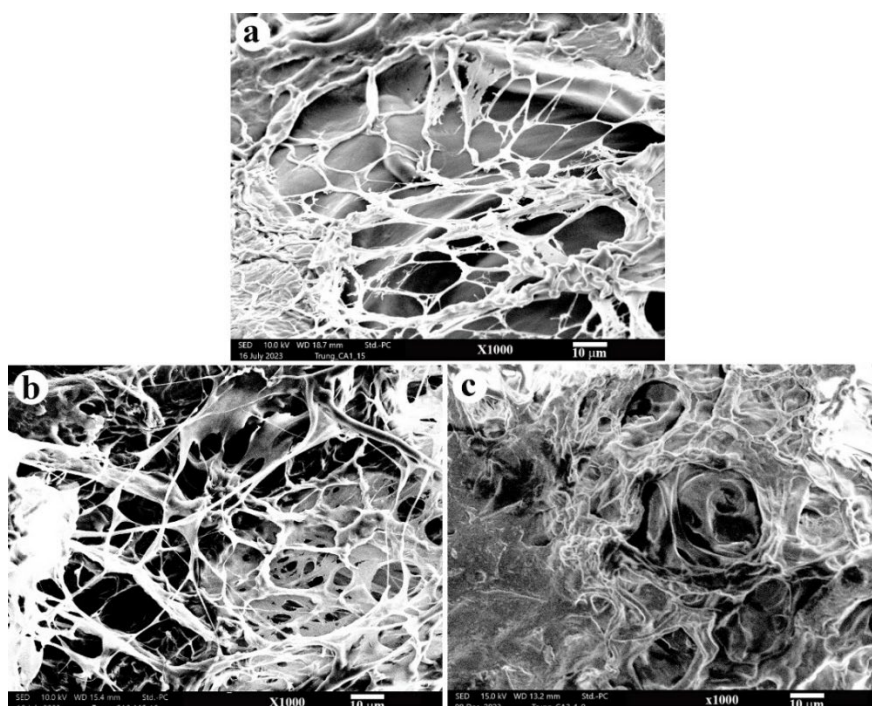


Figure 2: SEM images of CA1 (a), CA2 (b), and CA3 (c)

These results align with the cellulose standard (JCPDS no. 50-2241) and PVA standard (JCPDS no. 53-1847). A notable difference is the presence of a peak at 26.6° in the CA2 XRD pattern, which is characteristic of AC.

The crystallinity index of the samples was calculated, yielding values of 50.1% for CA1 and 76.4% for CA2. This increase in crystallinity index suggests that the chemical and thermal stability of CA2, which contains AC, is significantly higher than that of CA1. This indicates that doping with AC enhances the durability of the cellulose aerogel.

The adsorption band spectra of cellulose functionalized fibers, PVA, and CA samples were measured and are presented in Figure 4. For cellulose, the absorption band at 3273 cm^{-1} represents the stretched hydroxyl group (-OH) within the cellulose. Additional absorption bands are observed at 2941 cm^{-1} (symmetric and asymmetric $-\text{CH}_2$ groups in the glucose unit), 1730 cm^{-1} (C=C), and 1097 cm^{-1} (C-OH), which are consistent with previous research findings.^{13,30} The absence of adsorption bands related to the C-O stretching of hemicelluloses, C-C aromatic rings, and the distortion of C-H in the methyl, methylene, and methoxyl groups of lignin indicates that most hemicelluloses and lignin were removed during chemical treatment. For the CA samples, the

spectra show no significant differences compared to each other. The peaks are more intense and clearer than those of the cellulose sample. The absorption band at 3334 cm^{-1} (-OH) exhibits prolonged vibration due to hydrogen bonds within and outside the molecule. Additionally, absorption bands appear at 1714 cm^{-1} , 1417 cm^{-1} , 1375 cm^{-1} , and 1236 cm^{-1} , corresponding to the stretching vibrations of the C=O group, bending vibrations of the $-\text{CH}_2$ and $-\text{CH}_3$ groups, and vibrations of the -OH group, indicating the presence of PVA in the CA samples. Furthermore, strong adsorption bands at 2918 cm^{-1} and 2852 cm^{-1} are linked to the extended $-\text{CH}_2$ groups. FTIR analysis also confirms enhanced hydrophobicity of the CA material, evidenced by absorption bands at 1088 cm^{-1} and 825 cm^{-1} , which indicate the presence of silica Si-O bonding.¹¹

The results of the thermogravimetry analysis (TGA) and differential scanning calorimetry (DSC) of the CA2 sample are presented in Figure 5. In the temperature range of $70\text{--}120^\circ\text{C}$, approximately 7% of the mass was lost, likely due to the removal of water in the CA2. In the subsequent temperature range, there is no significant change in the mass of the CA2. However, above 210°C , the mass of the CA2 decreases sharply, indicating the decomposition of CA2 and the decomposition of PVA (which occurs

above 200 °C). This is accompanied by a substantial heat release, as shown by the DSC (heat flow) curve, suggesting a strong exothermic reaction. The heat flow curve shows a significant elongation in the temperature range of 400-600 °C,

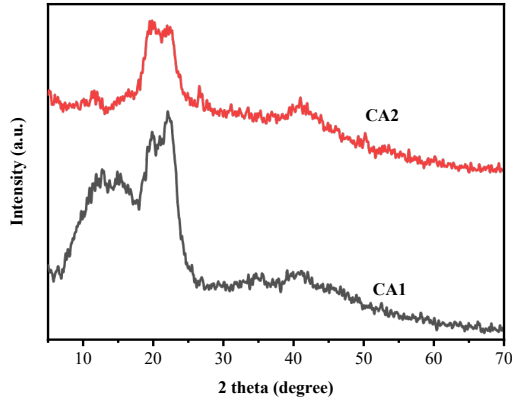


Figure 3: XRD patterns of CA1 and CA2

which can be attributed to structural changes and crystallization within the CA2, specifically the transformation of amorphous carbon into graphite.²³

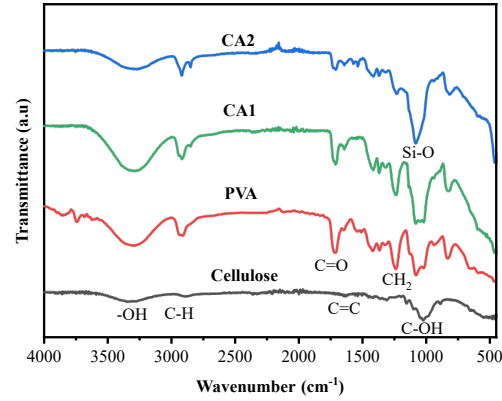


Figure 4: FTIR spectra of cellulose functionalized fibers and CA samples

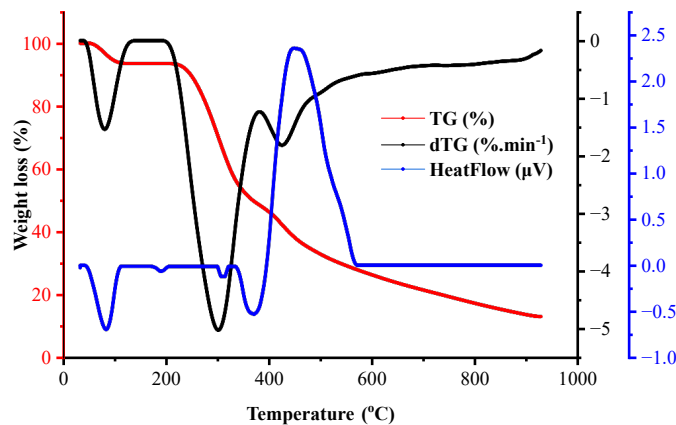


Figure 5: TGA-DSC curves of CA

The mass of CA2 continues to decrease, but slows down above 500 °C. This is due to the presence of activated carbon (AC) within the CA2, which is highly heat-stable and does not burn, generate heat, or decompose. Despite some similarities to previous studies in the thermal decomposition trend of the CA sample, the weight loss is not significantly reduced. At 900 °C, the sample has not reached its minimum mass, with about 13% of the original mass remaining, which is relatively high compared to previous studies.^{24,25} This indicates that the synthesized CA2 material has excellent thermal stability and could be used for oil spill treatment under harsh conditions or high temperatures, where traditional sorbents (polyurethane-based or polyethylene-based

materials) may fail.²⁶

The results of the N₂ adsorption-desorption isotherm at -196 °C, along with the surface area and pore size distribution graphs of the CA2 sample, are presented in Figure 6. The adsorption-desorption isotherm (Fig. 6a) exhibits a type III adsorption profile, indicating the simultaneous formation of monolayers, bilayers, and additional layers, resulting in exponential adsorption enhancement.^{27,28} Using the multi-point plot and trendline with slope and intercept parameters (Fig. 6b), the constant C is determined to be 5.635. From this, the surface area of the material is calculated to be 34.53 m²/g, the total micropore volume is 0.040 cc/g, and the porosity is 96.4%. The BJH pore size distribution plot (Fig. 6c) shows that the pores are

primarily distributed in the range of 17–60 Å, with an average pore diameter of 28.2 Å. The relatively low specific surface area of the material is attributed to the solid nature of the bagasse component, which has few pores. However, the

addition of activated carbon significantly improves this characteristic, yielding better results compared to previous studies on sugarcane bagasse aerogels.²⁹

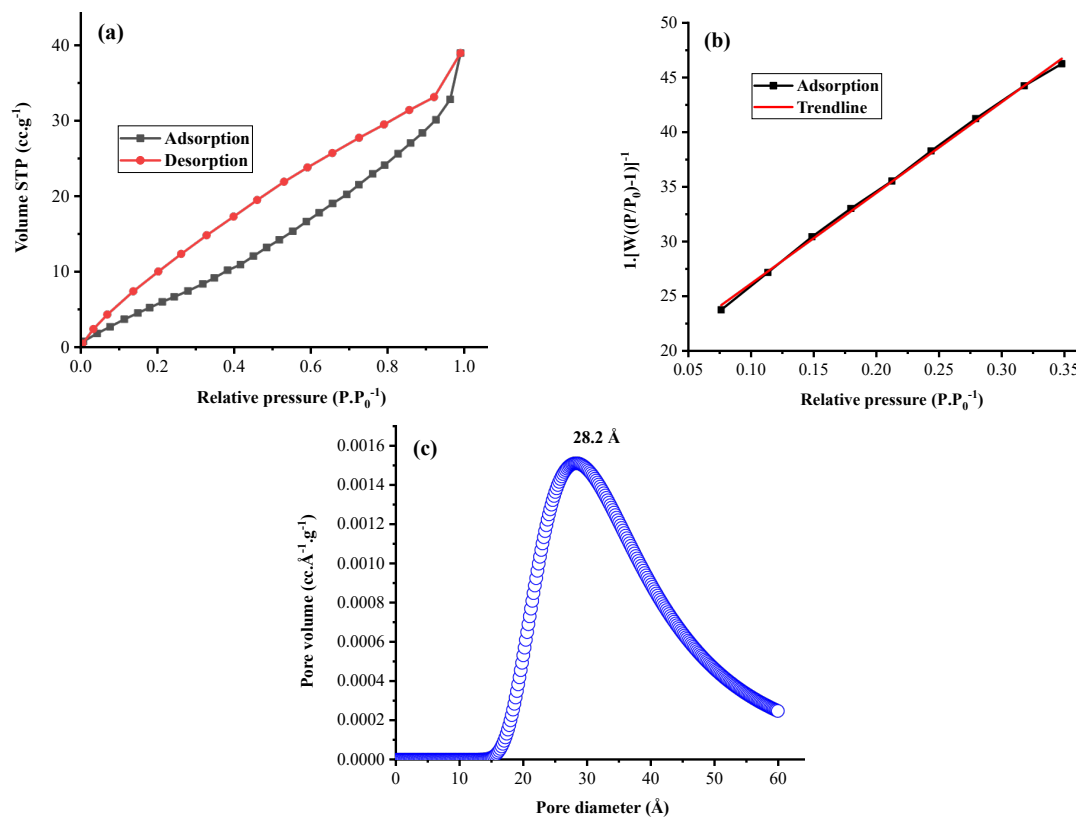


Figure 6: (a) N₂ adsorption-desorption isotherm curve; (b) Multi-point BET plot; (c) BJH pore size distribution adsorption curve

Oil spill tests

Salinity investigation

The effect of NaCl concentration in seawater on the CA samples is presented in Figure 7. The results indicate that increasing the NaCl concentration from 2.5% to 5.0% does not significantly alter the adsorption capacity, which remains stable at 8.29 g/g for CA1 and 12.78 g/g for CA2. This stability suggests that variations in salinity do not influence the adsorption performance of the material, likely because changes in salt concentration do not significantly affect the pH of the environment. Given that the average salinity of seawater is approximately 3.5%, we selected a NaCl concentration of 3.5% for other related experiments to ensure practical relevance and consistency in evaluating the material's performance under typical marine conditions. Consequently, the material demonstrates high adaptability for oil spill

treatment in seawater with varying salinity levels, without compromising efficiency.

Temperature and adsorption time investigation

The effect of temperature on the oil adsorption capacity of the aerogel samples was investigated, as shown in Figure 8(a), with 30 °C identified as the optimal temperature for adsorption. The experimental results indicate that in the temperature range of 10 °C to 30 °C, the adsorption capacity increased for both samples. However, beyond 30 °C, a decline in adsorption capacity was observed as the temperature increased. This trend can be attributed to the simultaneous occurrence of adsorption and desorption processes. Below 30 °C, the adsorption process dominates, leading to increased oil uptake. In contrast, at temperatures above 30 °C, the desorption process accelerates, reducing overall adsorption efficiency. Specifically, for the CA1 sample, the adsorption

capacity increased from 3.95 g/g at 10 °C to a maximum of 8.29 g/g at 30 °C, followed by a gradual decline up to 60 °C. Similarly, the CA2 sample exhibited a superior adsorption performance, with capacity rising from 9.19 g/g at 10 °C to a peak value of 12.78 g/g at 30 °C before

decreasing at higher temperatures. These findings indicate that 30 °C is the optimal temperature for maximizing oil adsorption efficiency and that the observed temperature dependence follows a trend similar to that of adsorption time.

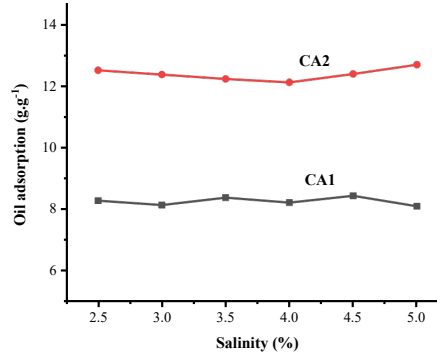


Figure 7: Effects of salt concentration on oil adsorption capacity

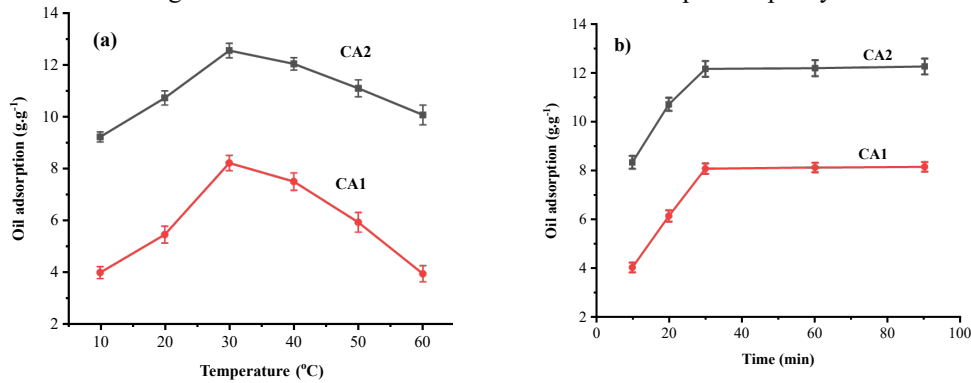


Figure 8: (a) Effects of temperature on oil adsorption capacity; (b) Effects of time on oil adsorption capacity

The effect of adsorption time on the oil adsorption capacity of the aerogel samples was investigated at room temperature, as shown in Figure 8(b). The experimental results indicate that adsorption capacity was measured at time intervals of 10, 20, 30, 60, and 90 minutes. The results demonstrate that the CA2 sample, which contains activated carbon, exhibited a significantly higher oil adsorption capacity compared to the CA1 sample without activated carbon. This finding suggests that the incorporation of activated carbon enhances the adsorption performance of the aerogel material. For both samples, a rapid increase in adsorption capacity was observed during the first 30 minutes, which can be attributed to the rapid filling of the porous structure with oil molecules. This fast initial adsorption occurs due to the strong attraction between the oil and the material's surface, driven by oleophilic interactions and capillary forces, which help the oil

spread and adhere to the surface quickly. Following this initial phase, oil gradually moves into the internal pores through van der Waals forces. As the adsorption process continues, the rate slows down as the available adsorption sites in the aerogel become occupied, leading to equilibrium.

Specifically, the adsorption capacity of CA1 increased from 4.24 g/g at 10 minutes to 8.34 g/g at 90 minutes, while CA2 exhibited a higher adsorption capacity, rising from 8.58 g/g at 10 minutes to 12.78 g/g at 90 minutes. In both cases, the adsorption process reached its peak at 30 minutes, after which the capacity remained relatively stable up to 90 minutes. These results confirm that activated carbon plays a crucial role in enhancing oil adsorption and establish 30 minutes as the optimal adsorption time for further studies.

Reusability investigation

The reusability of the aerogels was assessed by measuring the oil adsorption capacity of CA1 and CA2 over multiple reuse cycles. As shown in Figure 9, the adsorption capacity exhibited a sharp decline after the second cycle, followed by a gradual decrease in subsequent cycles. This reduction in performance is primarily attributed to structural changes occurring during repeated adsorption and desorption cycles, which likely result in pore deformation and reduced adsorption efficiency.

In the first cycle, CA1 exhibited an adsorption capacity of 8.26 g/g, while CA2 demonstrated a significantly higher capacity of 12.78 g/g, indicating its superior initial oil adsorption ability. However, in the second cycle, adsorption capacity

decreased sharply to 4.98 g/g for CA1 and 8.35 g/g for CA2. This decline may be due to incomplete oil removal and pore blockage during the regeneration process. From cycle 3 to cycle 5, both aerogels showed a continued, but more gradual decline in adsorption capacity. By the fifth cycle, CA1 retained initial adsorption capacity (4.11 g/g), while CA2 retained 7.91 g/g. The higher retention in CA2 suggests that it possesses better structural integrity and mechanical stability, allowing it to maintain more active adsorption sites over multiple reuse cycles. Overall, while both aerogels demonstrated reusability, CA2 exhibited greater durability and higher retention of adsorption capacity, making it a more suitable candidate for oil spill cleanup applications requiring multiple reuse cycles.

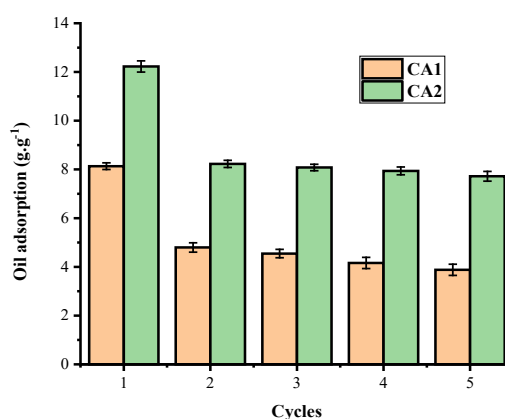


Figure 9: Reusability of CA1 and CA2

CONCLUSION

This study successfully synthesized aerogel materials from sugarcane bagasse using PVA as a cross-linking agent, combined with a freeze-drying method. The inclusion of AC in the aerogel matrix represents a novel enhancement compared to previous research. Utilizing simple chemicals and environmentally friendly methods, the study maximized the use of agricultural by-products. Modern analytical techniques revealed that the AC-doped aerogel possessed a uniformly distributed porous structure, particularly at a SB/PVA/AC ratio of 2:1:0.25. BET analysis indicated that the material exhibited type III adsorption characteristics, with a specific surface area of 34.53 m²/g and a total micropore volume of 0.040 cm³/g. The AC-doped aerogel was tested for its oil adsorption capability in marine environments under various conditions, including time, temperature, salinity, and reusability. Compared to undoped samples, the AC-doped

aerogel demonstrated significantly higher oil adsorption efficiency, with optimal performance at 30 minutes and 30 °C. The maximum adsorption efficiency was 12.78 g/g, surpassing previous studies on sugarcane bagasse-derived aerogels. This research marks a promising advancement in the development of aerogel materials, providing a foundation for future innovations.

ACKNOWLEDGEMENTS: The authors would like to express their sincere gratitude to the Technical Cooperation Project - Phase 2 (TC2), Japan for their financial support under the project number Model 6.

REFERENCES

- ¹ S. Wang, Y. He and M. Song, *J. Environ. Manage.*, **277**, 110999 (2021), <https://doi.org/10.1016/j.jenvman.2020.110999>
- ² M. Lorenzo and Y. Picó, *Curr. Opin. Environ. Sci. Health*, **9**, 77 (2019), <https://doi.org/10.1016/j.coesh.2019.05.007>

- ³ C. Liu, N. Bolan, A. U. Rajapaksha, H. Wang, P. Balasubramanian *et al.*, *Chinese Chem. Lett.*, **36**, 109960 (2024), <https://doi.org/10.1016/j.ccllet.2024.109960>
- ⁴ M. H. Saleem, M. F. B. Mfarrej, K. A. Khan and S. A. Alharthy, *Sci. Total Environ.*, **913**, 169755 (2024), <https://doi.org/10.1016/j.scitotenv.2023.169755>
- ⁵ S. Mishra, G. Chauhan, S. Verma and U. Singh, *Marine Pollut. Bull.*, **178**, 113609 (2022), <https://doi.org/10.1016/j.marpolbul.2022.113609>
- ⁶ G. G. Gagliardi, D. Borello, C. Cosentini, A. Barra Caracciolo, G. Aimola *et al.*, *J. Power Sourc.*, **613**, 234878 (2024), <https://doi.org/10.1016/j.jpowsour.2024.234878>
- ⁷ S. Muhammad, Y. M. Albadn, E. B. Yahya, S. Nasr, H. P. S. Abdul Khalil *et al.*, *Giant*, **18**, 100249 (2024), <https://doi.org/10.1016/j.giant.2024.100249>
- ⁸ Y. Dou, D. Tian, Z. Sun, Q. Liu, N. Zhang *et al.*, *ACS Nano*, **11**, 2477 (2017), <https://doi.org/10.1021/acsnano.6b07918>
- ⁹ M. Padaki, R. Surya Murali, M. S. Abdullah, N. Misdan, A. Moslehyani *et al.*, *Desalination*, **357**, 197 (2015), <https://doi.org/10.1016/j.desal.2014.11.023>
- ¹⁰ Q. B. Thai, S. T. Nguyen, D. K. Ho, T. D. Tran, D. M. Huynh *et al.*, *Carbohydr. Polym.*, **228**, 115365 (2020), <https://doi.org/10.1016/j.carbpol.2019.115365>
- ¹¹ G. Kumar, D. T. K. Dora, D. Jadav, A. Naudiyal, A. Singh *et al.*, *J. Clean. Prod.*, **298**, 126744 (2021), <https://doi.org/10.1016/j.jclepro.2021.126744>
- ¹² J. L. Gurav, I.-K. Jung, H.-H. Park, E. S. Kang and D. Y. Nadargi, *J. Nanomater.*, **2010**, 409310 (2010), <https://doi.org/10.1155/2010/409310>
- ¹³ T. T. Nguyen, N. T. Nguyen, V. V. Nguyen, A. H. Nguyen, B. D. H. Tran *et al.*, *Chemosphere*, **355**, 141748 (2024), <https://doi.org/10.1016/j.chemosphere.2024.141748>
- ¹⁴ Y. Sun, C. Deng and H. Dong, *Geoenerg. Sci. Eng.*, **240**, 213043 (2024), <https://doi.org/10.1016/j.geoen.2024.213043>
- ¹⁵ M. Jakob, A. R. Mahendran, W. Gindl-Altmutter, P. Bliem, J. Konnerth *et al.*, *Progress Mater. Sci.*, **125**, 100916 (2022), <https://doi.org/10.1016/j.pmatsci.2021.100916>
- ¹⁶ Z. Li, S. Lei, J. Xi, J. Huang, Z. Chen *et al.*, *Chem. Eng. J.*, **426**, 131245 (2021), <https://doi.org/10.1016/j.cej.2021.131245>
- ¹⁷ N. Ramirez, D. Zámbo, F. Sardella, P. A. Kißling, A. Schlosser *et al.*, *Adv. Mater. Interfaces*, **8**, 2100310 (2021), <https://doi.org/10.1002/admi.202100310>
- ¹⁸ T. Ahamad, M. Naushad, Ruksana, A. N. Alhabarah and S. M. Alshehri, *Int. J. Biol. Macromol.*, **132**, 1031 (2019), <https://doi.org/10.1016/j.ijbiomac.2019.04.004>
- ¹⁹ K. Okiel, M. El-Sayed and M. Y. El-Kady, *Egypt. J. Petrol.*, **20**, 9 (2011), <https://doi.org/10.1016/j.ejpe.2011.06.002>
- ²⁰ H. Yang, J. Sun, Y. Zhang, Q. Xue and S. Xia, *Ceram. Int.*, **47**, 33827 (2021), <https://doi.org/10.1016/j.ceramint.2021.08.294>
- ²¹ K. A. Tran, L. L. T. Nguyen, N. N. Huy, N. H. N. Do, K. A. Le *et al.*, *Int. J. Environ. Sci. Technol.*, **20**, 13717 (2023), <https://doi.org/10.1007/s13762-023-04960-3>
- ²² J. Feng, S. T. Nguyen, Z. Fan and H. M. Duong, *Chem. Eng. J.*, **270**, 168 (2015), <https://doi.org/10.1016/j.cej.2015.02.034>
- ²³ A. Onodera, K. Higashi and Y. Irie, *J. Mater. Sci.*, **23**, 422 (1988), <https://doi.org/10.1007/BF01174666>
- ²⁴ J. Li, L. Zheng and H. Liu, *J. Por. Mater.*, **24**, 1575 (2017), <https://doi.org/10.1007/s10934-017-0397-y>
- ²⁵ T. T. V. Nguyen, N. Tri, B. A. Tran, T. D. Duy, S. T. Nguyen *et al.*, *ACS Omega*, **6**, 26130 (2021), <https://doi.org/10.1021/acsomega.1c03137>
- ²⁶ Z.-Y. Wu, C. Li, H.-W. Liang, Y.-N. Zhang, X. Wang *et al.*, *Sci. Rep.*, **4**, 4079 (2014), <https://doi.org/10.1038/srep04079>
- ²⁷ X. Zheng, T. S. Ge and R. Z. Wang, *Energy*, **74**, 280 (2014), <https://doi.org/10.1016/j.energy.2014.07.027>
- ²⁸ M. A. Al-Ghouti and D. A. Da'ana, *J. Hazard. Mater.*, **393**, 122383 (2020), <https://doi.org/10.1016/j.jhazmat.2020.122383>
- ²⁹ Z. Li, S. Lei, J. Xi, D. Ye, W. Hu *et al.*, *Chem. Eng. J.*, **426**, 129580 (2021), <https://doi.org/10.1016/j.cej.2021.129580>